Journal of Micromechanics and Microengineering

ACCEPTED MANUSCRIPT

Critical analysis of micro-thermogravimetry of CuSO₄.5H₂O crystals using heatable microcantilevers

To cite this article before publication: Nikhilendu Tiwary *et al* 2019 *J. Micromech. Microeng.* in press https://doi.org/10.1088/1361-6439/ab30a3

Manuscript version: Accepted Manuscript

Accepted Manuscript is "the version of the article accepted for publication including all changes made as a result of the peer review process, and which may also include the addition to the article by IOP Publishing of a header, an article ID, a cover sheet and/or an 'Accepted Manuscript' watermark, but excluding any other editing, typesetting or other changes made by IOP Publishing and/or its licensors"

This Accepted Manuscript is **© 2019 IOP Publishing Ltd**.

During the embargo period (the 12 month period from the publication of the Version of Record of this article), the Accepted Manuscript is fully protected by copyright and cannot be reused or reposted elsewhere.
As the Version of Record of this article is going to be / has been published on a subscription basis, this Accepted Manuscript is available for reuse under a CC BY-NC-ND 3.0 licence after the 12 month embargo period.

After the embargo period, everyone is permitted to use copy and redistribute this article for non-commercial purposes only, provided that they adhere to all the terms of the licence https://creativecommons.org/licences/by-nc-nd/3.0

Although reasonable endeavours have been taken to obtain all necessary permissions from third parties to include their copyrighted content within this article, their full citation and copyright line may not be present in this Accepted Manuscript version. Before using any content from this article, please refer to the Version of Record on IOPscience once published for full citation and copyright details, as permissions will likely be required. All third party content is fully copyright protected, unless specifically stated otherwise in the figure caption in the Version of Record.

View the article online for updates and enhancements.

This content was downloaded from IP address 132.77.21.217 on 14/07/2019 at 08:22

IOP Publishing Journal Title
Journal **XX** (XXXX) XXXXXX https://doi.org/XXXX/XXXX

Critical analysis of Micro-Thermogravimetry of $CuSO_4.5H_2O$ crystals using heatable Microcantilevers

Nikhilendu Tiwary[1], Marjan Zakerin[2], Filipe Natalio[3], Eugen Biegler[4], Fritzsche Marco[4], Hermann Kaubitzsch[5], Apurba Laha[1], Rüdiger Berger[2], V. Ramgopal Rao[1]

[1] Department of Electrical Engineering, Indian Institute of Technology Bombay, Mumbai 400076, India
[2] Physics at Interfaces, Max Planck Institute for Polymer Research, Mainz 55128, Germany
[3] Institut für Chemie, Martin-Luther-Universität, Halle (Saale) 06120, Germany (until 31.07.17)
[4] Polytec GmbH, Waldbronn 76337, Germany
[5] BGK Infrarotservice GmbH, Riesa 01591, Germany

E-mail: berger@mpip-mainz.mpg.de, rrao@ee.iitb.ac.in

Received xxxxxx
Accepted for publication xxxxxx
Published xxxxxx

Abstract

Micro/nano thermogravimetry (TG) employing MEMS has significant potential to improve the minimum sample mass and mass resolution as compared to commercial TG instruments. Although there have been a few previous reports on MEMS TG, none of them have critically analysed the obtained TG curve in detail. In this work, we have designed and fabricated a microelectromechanical thermogravimetric device (MMTG) with integrated microheaters and temperature sensors. The mass sensitivity of the device was estimated to be 0.89 pg/Hz which outperforms the standard TG approaches. We tested the MMTG performance with $CuSO_4.5H_2O$ crystals. The final mass loss ratio corresponds to the theoretically expected value, although the obtained TG curve deviated from the standard TG curve of $CuSO_4.5H_2O$ obtained from commercial TG instruments. We attributed the deviation to the inherent temperature non-uniformity, non-isothermal conditions and temperature gradients of metallic-wire based microheaters. Finite Element (FE) simulations were carried out in order to confirm and gain insights into the non-uniform heating phenomena of microheater and sample. Based on the simulation results, we propose designs that can be realized to make MEMS TG a successful enterprise.

Keywords: Microcantilevers, Microheaters, Finite Element Analysis, Laser Doppler Vibrometer, Thermogravimetry

1. Introduction

Accurate temperature calibrations of microheaters are a daunting task and recent report by Gao *et al*. has outlined its difficulty [1]. Nevertheless, the temperature accuracy and calibration of MEMS heaters are extremely important. For example, precise control of temperature is essential for electrothermally driven microactuators [2] and polymerase chain reaction (PCR) based devices [3]. It is also the foremost criteria for realizing the overwhelming merit of MEMS heaters, *viz.* low thermal mass, fast thermal response and easy integration for intended applications. We have designed and fabricated a micromechanical cantilever sensor with integrated heater element to achieve a fast thermal response. With such a micro-heater element, samples can be

 © xxxx IOP Publishing Ltd

Accepted Manuscript

heated up to several hundred °C and cooled down to room temperature within a few milliseconds, thus making MEMS based thermogravimetry (TG) as an attractive device, especially for analysis of minute amount of samples. In this respect, it is very important to know and understand temperature calibration of MEMS based TG devices. Micro/Nano TG with MEMS involves interplay among individual components, such as microheaters, temperature sensors, frequency sensors and actuators. It has been observed that TG data obtained from MEMS based tools deviate from the one obtained from commercial TG instruments [4]. We have revisited MEMS based TG and fabricated a simplified device to overcome integration complexities. The majority of our effort is focussed on the temperature calibration, critical analysis of the obtained TG curve and understanding of the phenomena playing a role upon heating.

Thermogravimetry (TG) is a standard technique for analysing chemical compositions based on measured weight losses of samples with respect to an applied thermal budget. TG instruments work on a simple principle: a sample is loaded on a balance while the environment of the sample is controlled, e.g. an inert (He, N_2, ambient air) or a reactive atmosphere (CO, O_2). The sample is heated inside the furnace, and once reaching a specific temperature, the sample decomposes and gaseous reaction products form. The latter results in a mass loss of the sample which is measured by the balance. The final plot is weight loss versus temperature. The decomposition temperature and corresponding magnitude of weight loss give insights into the chemical composition of the sample.

Typically, the minimum sample mass which can be analysed by a commercial TG instrument is 1 mg and the mass resolution offered is of the order of 0.1 µg [5]. However, there are certain applications in which the minimum sample mass and mass resolution should be further reduced. This includes TG of various metal oxide nanowires [6-7], biomolecules [8-10] and forensics [11] which will yield more insights with a reduced sample mass and higher mass resolution as compared to the conventional counterparts.

In order to enable the TG analysis of nanogram samples, MEMS based tools have been developed. One of the easiest ways to realize a miniaturized balance is a micromechanical cantilever resonator. Its fundamental mode resonant frequency is given by: $f_0 = \frac{1}{2\pi}\sqrt{\frac{k}{m^*}}$ (1)

where, k is the spring constant and m^* is the effective mass of the microcantilever. For rectangular cantilevers $m^* = 0.24\ m_c$, where m_c is the mass of the micromechanical cantilever. Typical values for m_c range from 100 to 500 ng. At the end of the cantilever, a sample with mass M can be placed, which will change the resonant frequency to

$$f_m = \frac{1}{2\pi}\sqrt{\frac{k}{m^*+M}} \quad (2)$$

When the sample is heated, a mass change $M(T)$ results in a resonant frequency change $f_{TG}(T)$ of the resonator

$$f_{TG}(T) = \frac{1}{2\pi}\sqrt{\frac{k(T)}{m^*(T)+M(T)}} \quad (3)$$

Please note that k and m^* are also temperature dependent owing to the changes in Young's modulus and density of the cantilever material [12-13].

MEMS based cantilever devices are well known in literature with applications ranging from gas [14], chemical [15] and bio sensors [16]. With it masses down to the level of femtogram [17], attogram [18] and zeptogram [19] have been detected. Polysilicon piezoresistive microcantilevers were employed to perform TG of 0.4 µg of $CuSO_4.5H_2O$ [20-21] and a zeolite crystal ZSM-5 loaded with p-nitroaniline [22]. The polysilicon piezoresistor acted as heater and simultaneously as a sensor to detect changes in the resonant frequency. Ono *et al.* demonstrated TG of octavinylsiloxane by employing two microcantilevers (one for sensing and the other for reference) which were mounted on a heating stage inside a vacuum chamber. The resonant frequencies were recorded with the help of a double beam laser Doppler vibrometer (LDV) [23]. Lee *et al.* fabricated a microcantilever hotplate with integrated piezoresistors for resonant frequency sensing [24]. They were able to demonstrate TG of nanogram samples of paraffin. They employed MEMS devices allowing both optical detection as well as with integrated piezoresistive sensors [25]. In all of the above reports, the actuation of the microcantilever device was realized by piezoelectric or electrostatic actuation. Such an external actuation also has a possibility to induce non-linearity in the resonant frequency, when operated at higher excitation voltages [26]. In order to avoid this, direct drive methods have been applied. Toffoli *et al.* realized actuation of microcantilever hotplates by a frequency modulated red laser beam focused at the anchor of the device. Hereby, TG of 3.3 ng polyurethane was performed [4]. Lee *et al.* performed microthermogravimetry of a single microcapsule using silicon microcantilevers by measuring the thermal noise [27]. Recording the thermal noise spectra of cantilevers omits actuation of the cantilever sensor. An external heater was employed to heat the samples similar to [23]. Iervolino *et al.* fabricated an all-in-one device consisting of microheaters, temperature sensors, integrated piezoresistors as frequency sensors and integrated thermal actuators [28]. They were able to demonstrate TG of polyamide 6 and paraffin samples. But complexities in the fabrication process will tend to increase the overall cost of the device in a practical scenario. Therefore, in order to keep the MEMS device as simple as possible, while not sacrificing performance, only the minimum required elements should be integrated in the MEMS device.

Accepted Manuscript

Resonant frequency of microcantilevers also depends on the temperature (Eq. 3) [4,20,23,25,27-28]. Such resonant frequency changes add to those, which are induced by the mass loss of the sample. In order to compensate such a background, relative measurements were performed between loaded and unloaded microcantilevers [4,20,23]. Recently, Voiculescu *et al.* developed diamond cantilevers owing to the minimal dependence of its resonant frequency with temperature. With these cantilevers, TG of $CaCO_3$ crystals in the picogram range up to temperatures of 600 °C was performed [29]. Hereby, the heating of the cantilever samples assembly was carried out inside a thermal oven and the resonant frequency was recorded as the thermomechanical noise spectra with LDV. As heating of the sample was realized in an oven, it was as slow as standard TG. Thus, the main advantage of an integrated heater based microcantilever device, which is the fast thermal response, was sacrificed.

One of the main advantages of MEMS based TG is that sample weights down to sub-nanograms can be investigated. Moreover, in the case of MEMS based TG with in-built microheaters, temperature is a significant parameter and its accuracy in the microscale is important for good TG results. Toffoli *et al*. outlined that MEMS based TG is able to detect the mass change of single microcapsules, which can deviate significantly from standard TG that senses the average mass loss of many microcapsules [4].

Now for two decades, limited efforts are carried out [4,20-23,25,27-29] for the realization of MEMS TG. The major three drawbacks raised in literature are: (i) thermally induced resonant frequency shifts [4,20-21,23,25,27-28], (ii) thermal drift in integrated frequency sensors [20-21, 28], (iii) use of glue to fix samples on the cantilever [20-22] when actuation is employed and (iv) accuracy of temperature measurement.

In this report, we have tried to overcome all these listed problems and have revisited MEMS based TG. We performed thermogravimetry of $CuSO_4.5H_2O$ crystals using a micromechanical cantilever which is designed and fabricated in-house, and critically analysed the obtained TG curve in detail. We discuss sources of measurement errors and outline necessary improvements.

2. Our Approach

In the present work, we have designed and fabricated the micromechanical cantilever sensor with integrated heater element to achieve a fast thermal response. With such a micro-heater element, the sample can be heated and cooled down within a few milliseconds [24]. Subsequently, the frequency (~function of weight) measurement can then be performed at the same temperature, e.g. room temperature. This concept has the advantage that any other device parameters which may depend on temperature, remain unchanged during the weighing measurement. In particular, the present method eliminates the errors incurred by the temperature-induced changes of the Young's modulus or density. Further, no special material such as diamond would be required for fabricating microcantilevers. Thus, adapting our design enables us to simplify equation (3) as follows,

$$f_{TG}(T) = \frac{1}{2\pi}\sqrt{\frac{k}{m^* + M(T)}} \quad (4)$$

So, $M(T)$ can be expressed from (1) and (3) as:

$$M(T) = \frac{k}{4\pi^2}\left(\frac{1}{f_{TG}(T)^2} - \frac{1}{f_0^2}\right) \quad (5)$$

The mass loss ratio, i.e. *M(T)/M* can be calculated as:

$$\frac{M(T)}{M} = \frac{\left(\frac{1}{f_{TG}(T)^2} - \frac{1}{f_0^2}\right)}{\left(\frac{1}{f_m^2} - \frac{1}{f_0^2}\right)} \quad (6)$$

The above equation eliminates the need for individual calibration of spring constant of the devices. In order to keep the device as simple as possible, we discarded the integrated deflection sensors and mechanical actuator for driving the cantilever into resonance. Employing a mechanical actuator may result in large amplitude of oscillation. Therefore, glue was used to fix samples to prevent them from moving or falling off in literature [10,20-22]. However, if the decomposition temperature of glue is within the temperature range of a sample's TG curve, then it will interfere and contribute to the TG signal. In order to avoid displacements of samples, low amplitudes of oscillation are required. The lowest one is given by the thermal displacements of a microcantilever which is typically in the order of picometers. Therefore, we have measured the thermomechanical noise spectra using a highly sensitive LDV to determine its resonant frequency.

3. Design and Fabrication of MEMS TG device

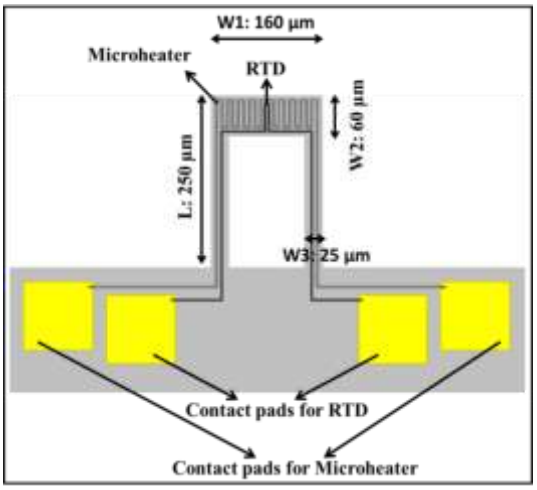

Fig. 1 Layout/design of U-shaped MMTG device with the dimensions (size of gold contact pads is reduced for clarity).

For TG we have integrated a microheater and resistance temperature detector (RTD) onto a U-shaped microcantilever (Fig. 1). This type of geometries was already employed in the past [30]. We considered it in order to overcome

Accepted Manuscript

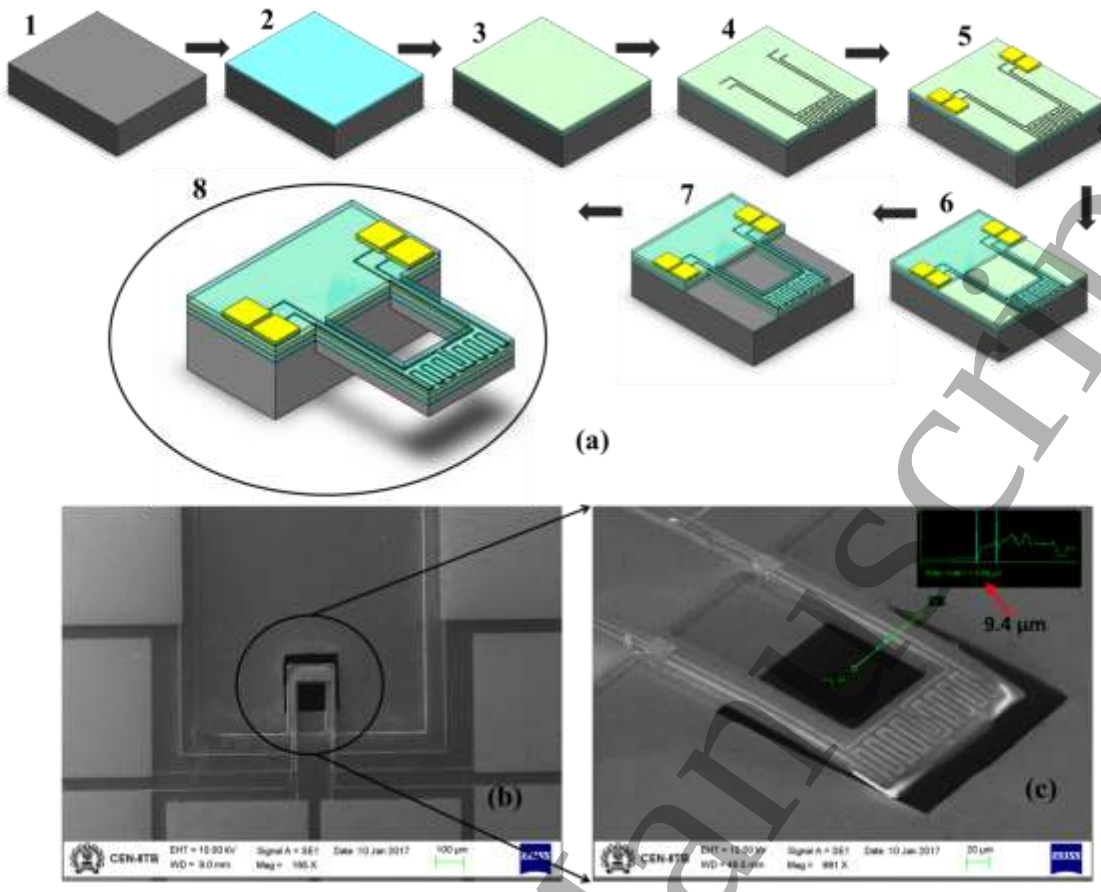

Fig. 2 (a) Fabrication process flow of the devices: (1) RCA cleaned silicon substrate (2) wet oxidation (SiO_2 ~ 1000 nm), (3) Silicon nitride deposition by ICPCVD (~ 1000 nm), (4) Patterning of Microheater and RTD, (5) Deposition and patterning of gold contact pads, (6) Encapsulation layer deposition and patterning, (7) Front side nitride & oxide etch and (8) back side etching and release, (b) and (c) SEM micrographs of the fabricated device.

undesired complexities in the fabrication process. The dimensions of the device are selected considering easy integration of microheater and RTD, sufficient area for mounting of test samples and ease of fabrication. The width of the microheater is kept as 4 µm and that of RTD as 3 µm.

The fabrication of microelectromechanical thermogravimetric (MMTG) device consists of a 5 mask process. It starts with an RCA (Radio Corporation of America) cleaned P-type double-sided polished (DSP) silicon wafer with orientation (100) and resistivity 4 – 7 ohm-cm. After the standard cleaning protocol, wet oxidation was carried out to grow silicon dioxide of thickness 1 µm. Deposition of silicon nitride of thickness ~ 1 µm was carried out on top of the oxide, using inductively coupled plasma – chemical vapour deposition (ICPCVD) using SiH_4 and N_2 as a precursor gas. This technique is typically used for obtaining high quality Si_3N_4 films with low hydrogen content [31-32]. The microheater and the RTD (resistance temperature detector) were patterned using lithography and sputter deposition of Tantalum (*Ta*)/Platinum (*Pt*) of thickness 10/100 nm followed by lift-off. *Ta* acts as an adhesion layer for *Pt* and is shown to be stable for temperatures ≈ 950 °C [33]. Similarly, contact pads were patterned and Chromium (*Cr*)/Gold (*Au*) of thickness 10/100 nm were deposited for making contact to the microheater and RTD. Encapsulation of microheater area was carried out with deposition and patterning of sputtered silicon dioxide of thickness 250 nm. After this, front side nitride and oxide were patterned and etched in plasma created with ~10:1 flow ratio of CHF_3/O_2 respectively to expose the underlying silicon from top. Etch windows were patterned from the bottom and thermal oxide was etched in 1:5 Buffered oxide etch (BOE) to expose the silicon. Finally, devices were exposed to Tetramethyl ammonium hydroxide (TMAH) solution for etching out the silicon for release of the devices. Fig. 2 (a) shows the detailed fabrication process steps and Fig. 2 (b)-(c) show SEM images of a fabricated device.

It is well known that silicon dioxide and silicon nitride develop stress across the length of the microcantilevers which results in bending of the beams [34]. Compensation of stress is often a challenge with various process adjustments and optimizations. Moreover, realization of thermogravimetric tests with bent microcantilevers and optical read-out is not easily feasible. Therefore, a layer of silicon is left intentionally below the oxide-nitride bilayer. This additional layer not only reduces the stress but also

Accepted Manuscript

increases the spring constant, resonant frequency and quality factor of the cantilever devices. Fig. 2(c) shows the thickness of one arm as 9.4 µm. Subtracting the thickness of SiO_2 (1 µm) and Si_3N_4 (1 µm), the thickness of silicon layer can be estimated to be 7.4 µm. The resonant frequency of the fabricated devices ranged from 180 kHz to 300 kHz which is attributed to the variation in the thickness of un-etched silicon beneath the beam. The device which was tested for TG (Fig. 2(b) and 2(c)) had a resonant frequency of 230 kHz. Its spring constant (k) was estimated by Finite Element (FE) simulations in COMSOL (S1 of supplementary information) and was found to be ≈ 216 N/m. The mass sensitivity of the device [35] was calculated according to:

$$S = \frac{k}{2\pi^2 f_0^3} \qquad (7)$$

By inserting k as 216 N/m and f_0 as 230.72 kHz, the mass sensitivity of the device was calculated to be 0.89 pg/Hz.

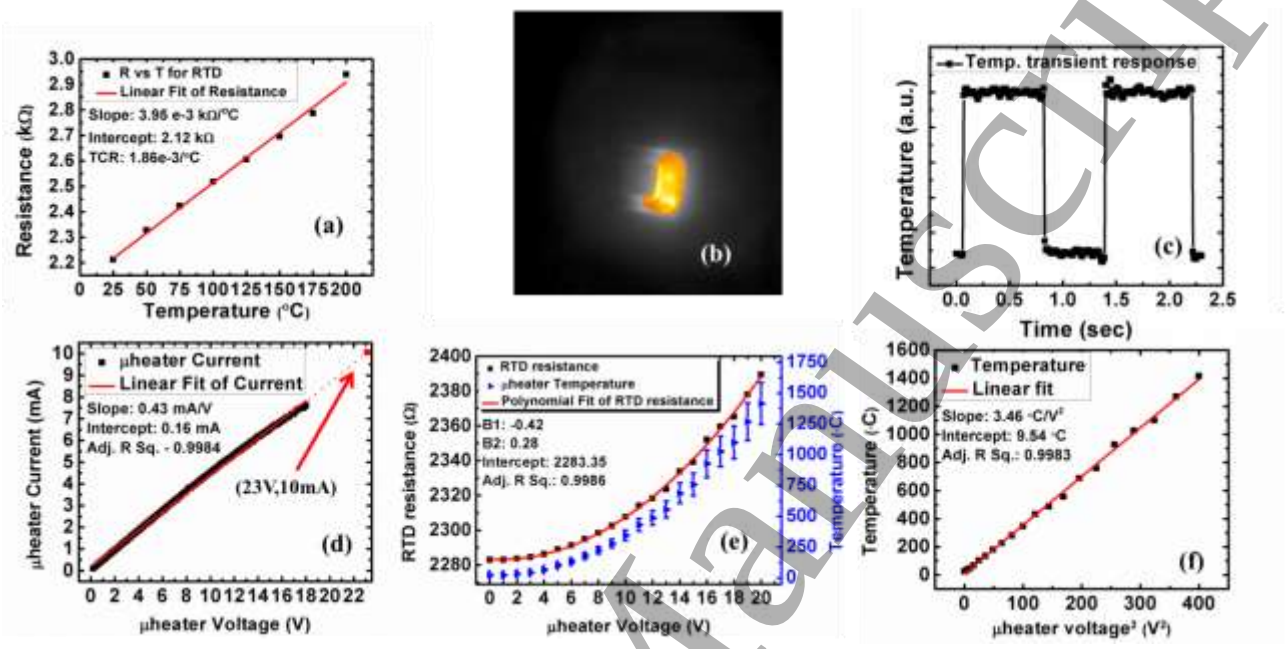

Fig. 3 (a) R versus T of RTD, (b) IR image of device showing the temperature distribution across the microheater platform, (c) Transient response of the microheater as extracted from IR camera (baseline corrected), (d) current – voltage characteristics of microheater, (e) Plot of RTD resistance and microheater temperature versus microheater voltage and (f) shows the linear plot of temperature versus (voltage)^2 with corresponding fit parameters. Utilizing these parameters, the temperature of the device at any particular voltage level can be estimated.

4. RTD and Microheater Calibration

For TG analysis, temperature is a salient parameter which determines the mass loss. Thus, calibration of microheaters and temperature sensors is a crucial aspect. In earlier reports [4,20-22,25], we have seen that changes in the resistance of the microheater itself can be used for temperature measurements. However, the resistance of the microheater is only accurate when the entire film is heated uniformly. In our case, the platinum wires are continuous until the gold contact pads. The wires are also situated in non-heated areas. Therefore, using the microheater as a temperature sensor for ultra-high temperature will not be accurate. Moreover, in the case of platinum microheaters there is a drift in its resistivity at high temperatures [36]. Instead, a separate RTD can be used for the calibration of microheater temperature. The RTD will be read-out at a low voltage whereas the microheater will be heated at higher voltage values, i.e. higher electrical power. Therefore, the RTD will not suffer from additional stress due to electromigration and thermomigration which occur at high voltage/temperature.

RTD: The RTD was characterized to extract its temperature coefficient of resistance (TCR) value on a hot chuck of a temperature dependent current-voltage (I-V) set up of Karl suss. The connections were done using Keithley 708A switching system matrix. The RTD was given a sweep voltage of – 0.5 to 0.5 V and the corresponding current values were extracted. From the recorded data, we calculated the temperature dependent resistance of RTD (Fig. 3(a)). The linear response shows the advantage of using platinum as the material owing to its inherent linear characteristics. The TCR of the RTD extracted was 1.86 x 10^{-3}/°C which is lower than the one for bulk platinum 3.9 x 10^{-3}/°C [37]. Lower TCR values for thin films are known and are attributed to a change in crystallinity and variations of the underlying adhesion layer [37]. The TCR values of Pt thin films are stable for a wide temperature range (reported till 800 °C) [33]. Moreover, the significant drift in the TCR values are only observed during degradation/burn out of Pt thin films [33]. In

Accepted Manuscript

conclusion, the RTD resistance depends linearly on temperature when heated on a hotplate.

Microheater: The microheater and RTD was mounted on a Printed Circuit Board (PCB) and connected to the conducting tracks using silver epoxy paste and hardener. We performed infrared (IR) imaging (camera model: FLIR A6753s) of the microheater area to confirm its functionality. IR imaging is useful for imaging the temperature profile across the heated platform and to identify hot spots [38-41]. When the heater is operated at 16 V, local hot spots across the microheater platform could be observed, Fig. 3(b). These hot spots correspond to ≈ 9–12 % of the average temperature across the platform. Such hot spots are reported for meander-shaped microheaters due to reduced electron mobility at corners of the meander [42]. The wavelength of the IR radiation at higher temperatures is typically < 1 µm which makes the accurate absolute measurement of temperature difficult owing to the typical larger wavelength (3-5 µm) capability of the IR camera. Moreover, in order to obtain the accurate temperature values, the emissivity of the device has to be known which is challenging for micrometer sized devices and its value changes at higher temperatures [43-45]. Therefore in our case, we could not accurately quantify the exact temperature but we have used the IR images for a relative evaluation of temperature profile and hot spots.

The transient response of the microheater device was studied using temporal plot from the graphical user interface (GUI) of IR imaging, for heating cycles/pulses of 1 sec duration (Fig. 3(c)). The time constant of the device capable of heating and cooling down was found to be < 10 msec as 10 msec was the framerate of the IR camera. The transient response shows that by applying short pulses, the microheater can be heated and cooled down within a fraction of a second. This in turn will avoid stress due to electromigration and thermomigration in the microheater due to a prolonged DC voltage, which would finally result in the failure of microheater elements [46].

We observed that for currents > 10 mA, the resistance of the microheaters suddenly increased to infinity. The microheaters were failing with a significant damage of the platinum films. We associate the current value at which the microheater fails to the melting temperature of platinum (1768 °C). The melting point of thin films for a general thickness >50 nm is equivalent to the bulk values [47-48]. We took the melting temperature and the corresponding power that led to failure of the heater as one calibration point (burn-through), and room temperature as second calibration point. Fig. 3(d) shows the current-voltage characteristics of the microheater from a Keithley 2400 source meter well below the melting temperature (current < 10mA) and thus harmless for the functionality of the heater. For simplicity we fitted a line to the data (red line in Fig. 3(d)). Then we extrapolated the line to 23 V (red dotted line) which corresponded to the current value of 10 mA.

To perform the calibration of RTD with microheater temperature, voltage steps were applied across the microheater in steps of 1 V (for 1 sec) by an Agilent E3641A DC power supply. The corresponding RTD resistance was monitored via a programmed GPIB to USB cable 82357B of Agilent Technologies from Keithley 2000 multimeter connected across the RTD. Fig. 3 (e) shows the RTD resistance values (black data points) recorded when voltage pulses were applied across the microheater of the device (left side of y-axis). A quadratic fit was obtained depicting that the temperature increase in the microheater was according to the power dissipation across it ($Power \propto V^2$). However, it is important to note that the measured RTD resistance value does not correspond to the temperature of the cantilever's sample platform. The RTD resistance value represents an average temperature value along the entire length of the RTD resistor length. Even the temperature profile at the sample platform is inhomogeneous (Fig. 3(b)).

Various reports outline that the RTD would sense a lower temperature due to the gap between the microheater and RTD [43]. The inherent thermal gradient due to non-uniform heating of platform is also reported to introduce errors in the accurate calibration of RTDs [44]. Therefore, in contrast to the hot plate experiment, the RTD value is used here as a sign for temperature but the measured resistance value (Fig. 3(e)) does not correspond to the heater temperature and also not to the sample temperature.

Therefore, we followed another approach: The average temperature realized by microheater can be calculated with RTD resistance change by the following equation.

$$T = \frac{R_{RTD} - R_{25°C}}{R_{25°C} \times \eta \times TCR} + 25 \ (in \ °C) \qquad (8)$$

Here, $R_{25°C}$ is the resistance of RTD at room temperature, R_{RTD} is the resistance of RTD at temperature T, η is the effective fractional length of RTD responding to the microheater temperature and TCR is the temperature coefficient of resistance of RTD. Thus, the expression $(R_{RTD} - R_{25°C})$ ensures the differential increase in RTD resistance due to microheater. η is the fractional ratio of RTD which actually respond to the microheater temperature. In order to calibrate the RTD resistance change with the microheater temperature, η has to be estimated. It was evaluated taking the burn-through calibration point (1768 °C). The corresponding RTD resistance at the burn-through voltage can be estimated by extrapolation of the fit (red curve in Fig. 3(e)). For 23 V (burn-through voltage), R_{RTD} was calculated to be 2424 Ω. Putting the values for T, R_{RTD}, $R_{25°C}$ & TCR as 1768 °C, 2424 Ω, 2283 Ω, 1.86 e-3 /°C respectively in Eq. 8; η was estimated to be 0.018. The total length of RTD is 1897.4 µm and the calibrated length of RTD corresponding to the above temperature of the microheater yields a value ≈ 34 µm (1.8%). Thus, only 34

Accepted Manuscript

µm of the RTD length can be assumed to virtually respond to the temperature acquired by the microheater according to the calibration method employed. Taking this into account and with the TCR obtained from Fig. 3 (a), the temperature acquired by the microheater can be calculated. Fig. 3 (e) shows the plot of microheater temperature (right side of y-axis) as a function of microheater voltage. The error bars corresponds to 12% of the average temperature as estimated from FLIR data of Fig. 3(b). Fig. 3 (f) shows the plot of V^2 *vs Temperature* across the microheater.

5. Thermogravimetry with $CuSO_4.5H_2O$ crystals

All the resonant frequency characterizations exploiting the thermomechanical noise spectra were done with a laser Doppler vibrometer MSA-100-3D capable of displacement measurements < 0.2 pm [49]. The measured thermomechanical noise spectrum was fitted with a Lorentzian curve. From the fit parameters, we took the resonant frequency and the Q-factor was obtained as a ratio of the resonant frequency and the 3dB bandwidth extracted from the fit data (bandwidth method). For an unloaded, pristine device we obtained a resonant frequency of 230.72 kHz ± 3 Hz and a Q of 216, Fig. 4 (a).

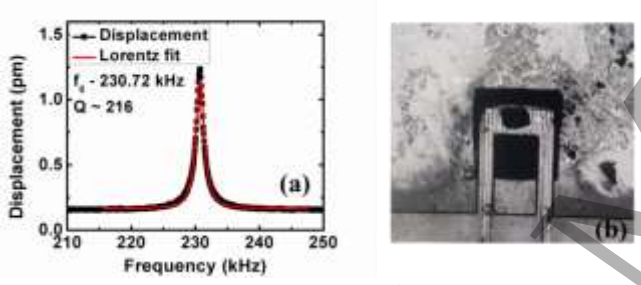

Fig. 4 (a) Thermomechanical noise spectra of the pristine device (without sample mounted), and (b) Optical image of the device with a piece of $CuSO_4.5H_2O$ mounted on it.

The $CuSO_4.5H_2O$ crystals were crushed into smaller pieces. One of the crystal pieces was then picked up and mounted at the center of the microheater platform by means of a micromanipulator. As the thermal displacement amplitude is quite small, the sample does not need to be fixed by glue or other means. Fig. 4 (b) shows the device mounted with a piece of $CuSO_4.5H_2O$. A subsequent recorded thermomechanical noise spectrum showed a decrease in resonant frequency to 93.23 kHz ± 73 Hz. The laser spot was focused on the device and not directly on the sample. Moreover, it was found that the resonant frequency recording of the device was independent of the position of laser spot across the heated platform. The mass of the sample mounted was calculated to be ≈ 527 ± 1 ng using Eq. 5.

For TG of the $CuSO_4.5H_2O$ sample, we applied n_{hp} = 5 voltage pulses (V_{hp}) at an interval of 1 second to the heater. Then, V_{hp} were increased successively in steps of 200 mV until a voltage of 16.4 V (T~940°C) was reached. The thermomechanical noise spectrum of the cantilever was recorded after the application of each voltage cycle.

Fig. 5(a) shows the shift in the resonant frequency (black data points) with respect to the applied voltage. The mass loss ratio of the copper sulphate crystal can be calculated according to Eq. 6. The temperature values at each of the voltage levels were calculated with the help of the fit parameters obtained from Fig. 3 (f). Fig. 5(a) (blue data points) and 5(b) (black data points) show the mass loss ratio obtained with our MMTG device versus voltage and temperature respectively. The horizontal error bars in temperature are calculated from the FLIR data which we estimated to be a maximum of 12%. We found that the mass loss ratio decreased from 100% to 70% until a nominal temperature of ≈ 500 °C was reached. Between 500 °C – 700 °C the ratio dropped further to 33%. From 700 °C – 940 °C, no further change in mass loss ratio was measured.

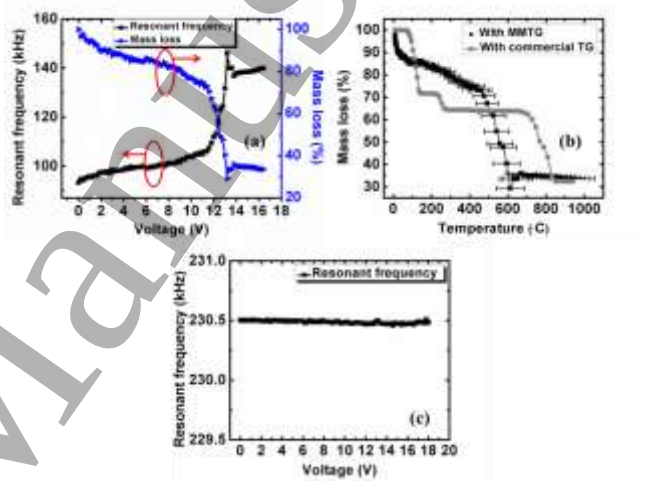

Fig. 5 (a) Resonant frequency/mass loss ratio versus applied voltage (b) Comparison of TG curve from MMTG device and commercial TG instrument (data points extracted from [48]) and (c) Plot of resonant frequency and Q-factor versus voltage of bare device.

The final mass (177±1 ng) corresponds to a mass loss of 33.6%. This mass loss indicates that $CuSO_4.5H_2O$ dehydrates completely and also reduced finally to Cu_2O following these reaction steps [48]

(I) $CuSO_4.5H_2O \rightarrow CuSO_4.3H_2O + 2H_2O$ (At T ~ 57–77 °C)
(II) $CuSO_4.3H_2O \rightarrow CuSO_4.H_2O + 2H_2O$ (At T ~ 77–117 °C)
(III) $CuSO_4.H_2O \rightarrow CuSO_4 + H_2O$ (At T ~ 187–247 °C)
(IV) $CuSO_4 \rightarrow CuO + SO_2 + 0.5O_2$ (At T ~ 600–780 °C)
(V) $4CuO \rightarrow 2Cu_2O + O_2$ (At T ~ 780–985 °C)

Although the final mass loss ratio corresponds to the theoretically expected value (≈ 32%), it is obvious that the experiment conducted with our device did not resolve these individual five reaction steps. For comparison, we plotted a TG curve of $CuSO_4.5H_2O$ crystals obtained from commercial TG instrument that was reported by Kunert (grey data points in Fig. 5(b)) [50].

The behaviour of the device without any sample mounted on top was recorded as reference (black data points in Fig. 5

Accepted Manuscript

(c)). The data shows that the thermally induced resonant frequency shifts are negligible. It also demonstrates that presence of moisture or any hydrocarbons on the cantilever material has no effect on the resonant frequency. Robert L.White studied intensively the dehydration of $CuSO_4.5H_2O$ in different environments [51]. He found that purging with Helium gas, the monohydrate is formed directly from the pentahydrate without resolving reaction steps (I) and (II). In our case, we performed the experiment in ambient air in a laboratory with air conditioning. Thus, water that is desorbed from the sample while heating is transported away by convection. The MMTG can also be brought inside a closed chamber, which can be purged with gas. Thus, the effect of reactive gases on the thermal decomposition can be studied as well. The aim of this manuscript is to critically discuss heating of micromachined devices. We believe that the current technology in heating is the dominating effect for the deviation in TG curve. The environment needs to be controlled for reliable calculation of the activation energies and determination of the crystal structures. However, compared to the heating issue, the latter is a secondary effect. Additional reactions of the $CuSO_4.5H_2O$ sample with SiO_2 and Pt are ruled out as a possibility. SiO_2 and Pt are unreactive and behave similar to the commercial TG pans (platinum or ceramic). Consequently, the TG curve recorded with the $CuSO_4.5H_2O$ samples is a purely temperature induced mass change.

We identified two major reasons for differences in the temperature induced mass change as compared to a commercial TG:

(a) In commercial TG instruments, the sample is placed inside an oven where it experiences a uniform temperature distribution across it. As we have reported here, the calibration of the RTD indicates inhomogeneous temperature distributions. We have estimated an error of 9-12% across the platform with IR results (Fig. 3(b)). This inhomogeneous heating is not only limited to the heater element but will result in inhomogeneous heating of attached samples which ultimately results in broadening of the above mentioned reaction steps. It is difficult to exactly quantify the temperature gradient across the sample in the actual scenario. However, it is worth to note from literature that, TG performed with in-built microheaters on microcantilevers shows dominant mass loss at temperatures preceded by ≈ 75 – 200 °C, before the intended temperature one gets from a commercial and conventional TG [4,25,28]. This implies that with in-built meander/non-bulk heaters, temperature gradients across sample are present which finally result in significant errors in temperature and hence, mass loss.

(b) In commercial TG instruments, the heating rate is linear (varies from ≈ 5 °C/min – 10 °C/min) or is even decreased to zero when mass changes occur as in the case of isothermal TG [52]. In the case of microheaters, we cannot directly define a heating rate owing to the < 10 msec transient response time. Thus, TG experiments performed under isothermal conditions yields a better mass and temperature resolution [52-53]. This is difficult to directly realize with a micromachined heater on a planar cantilever structure owing to its fast transient response time.

In conclusion, microcantilevers exhibit an essential improvement in mass resolution for TG, but temperature resolution offered by inbuilt microheater is poor. The mass sensitivity of the cantilever calculated using the standard formula, i.e. 0.89 pg/Hz, is the best which we could achieve from the cantilever, and that outperforms the mass sensitivity of the commercial TG instruments. However, due to the spatial non-uniformity in the temperature across heater platform and sample (as a result), as well as inherent non-isothermal condition offered by the in-built metallic-wire microheater, the temperature resolution is reduced which ultimately degrades the mass resolution. Thus, the drawbacks of metallic-wire based microheaters are (i) inherent temperature non-uniformity of microheater platform, (ii) non-uniform heating of the samples, (iii) formation of temperature gradients across test samples, and (iv) non-isothermal conditions. In order to make a step towards resolving all the minute reaction steps, we propose to realize the following conditions: (a) design heaters that allow a uniform temperature across the heated platform and sample, (b) methods to achieve isothermal heating.

(a) Uniform temperature across heated platform is difficult to realize with metallic microheaters due to the presence of hot spots at sharp corners, effects of electromigration and thermomigration at high temperatures. Moreover, electromigration and thermomigration is also pronounced with repeated cycles of heating. In order to overcome this issue bulk microheater elements can be used [54-55]. To explore this approach, we performed FE simulations in COMSOL with joule heating physics by creating three designs of microheaters (D1, D2 and D3) and studied the temperature uniformity across the platform as well as temperature gradients across a sample that was mounted on it (Fig. 6 and 7). All the material parameters were taken as in-built values (unless specifically mentioned). For D1, a meander Pt microheater of thickness 0.2 µm and width of 10 µm is formed with Au contact pads (Fig. 6a and 7a). For D2, a Poly-Si layer of resistivity 1e5 Ω-m and thickness 0.2 µm is formed with Pt as contact pads (Fig. 6b and 7b). In order to achieve better temperature uniformity, graded Poly-Si layers are formed in D3 (Fig. 6c and 7c) in which the resistance of different Poly-Si layers are varied. The layers of Poly-Si in union with the Pt contact pads are made relatively more resistive (1.05e5 Ω-m) than the middle Poly-Si layer (0.95e5 Ω-m). As the temperature in the middle of the platform is always higher, the grading was done to ensure higher power dissipation at the outer areas and relatively less power

Accepted Manuscript

dissipation in the middle layer. This will ultimately improve the temperature distribution across the platform [56]. The convective heat transfer coefficient of 10 W/m^2.K was applied to the heater layers for the three designs and the edges of the Si were set at room temperature (20 °C). Fig. 6 shows the temperature profiles and line graphs across the x-axis of the platform for the three designs for a power dissipation of 3 W. The FE simulations revealed that the temperature attained by Pt microheater (D1) is greater than bulk microheaters (D2 & D3). On the other hand, the temperature profile across D2, D3 is better as compared to D1. The percentage length at the middle of the platform along x-axis for which temperature is > 90 % of the peak value is ≈ 68 % & 77 % for D2 and D3 respectively.

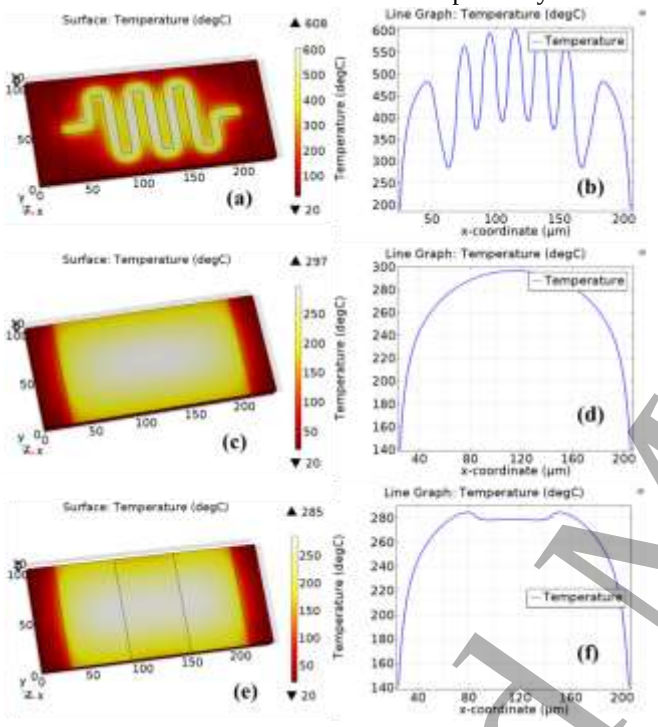

Fig. 6 FE simulation results for microheater platform: The microheater consists of a 230 µm (L) x 100 µm (W) x 10 µm (T) Si base on top of which there is SiO_2 (1 µm) and Si_3N_4 (1 µm). The contact pads of dimensions 25 µm x 100 µm x 0.2 µm were formed at the two ends of the platform for all the three designs. (a) D1: a meander microheater, (c) D2: a poly-Si heater (e) D3: graded poly-Si heater, and (b), (d), (f) temperature profile along x-axis for D1, D2 and D3 respectively for a power dissipation of 3 W.

Furthermore, we added a test sample of $CaCO_3$ on top of the platform and studied the temperature gradient across it at similar heater temperature (≈ 600 °C) attained by D1, D2 and D3 (Fig. 7(a,b,c)). The gradient across z-axis of the sample is 58 °C, 32 °C and 29 °C for D1, D2 and D3 respectively (Fig. 7(d)). Moreover, the temperature profile across the x and y-axis at top and bottom (in contact with heater) surface of the sample was also evaluated, which can be found out from supplementary information, S2. The temperature difference at the top surface of sample is negligible for all the three designs. The temperature difference is significantly greater at the bottom surface where the sample is in contact with the heater. Table 1 summarizes the difference between maximum and minimum temperature across the sample in x, y and z axes for the three designs. Our simulations indicate that a graded bulk microheater tends to attain and provide much better temperature uniformity across the heater platform and the sample. The TG results from reports which used in-built bulk heaters with better temperature uniformity [20] and external/oven-based heating [23, 29] matches somewhat well with the curve obtained from commercial TG instruments. This observation further reaffirms that heating of the sample with internal elements is a critical issue and needs to be addressed. Thus, a uniform temperature platform also ensures minimal temperature gradient across sample. Furthermore, novel heater architectures as one described in [57] could also be employed for uniform heating of samples with negligible temperature gradient across it.

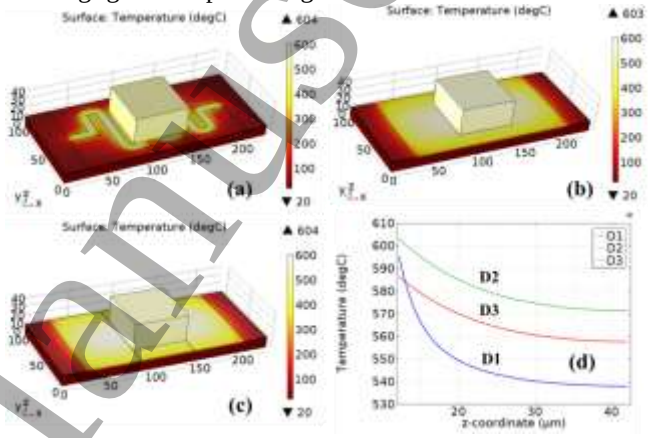

Fig. 7 FE simulation results for microheater platform with $CaCO_3$ sample: 60 µm (L) x 60 µm (W) x 30 µm (T) for (a) D1 meander microheater, (b) D2 poly-Si heater, (c) D3 graded poly-Si heater, and (d) temperature profile across the sample in z-axis for D1, D2 and D3 respectively.

Table 1. Maximum temperature gradient across sample in x, y and z directions for D1, D2 and D3 for temperature of ~ 600 °C.

	Z-axis (in °C)	X-axis (in °C)		Y-axis (in °C)	
	ΔT	ΔT: bottom surface of sample	ΔT: top surface of sample	ΔT: bottom surface of sample	ΔT: top surface of sample
D1	58	55	1	113	4
D2	32	9	1	99	7
D3	29	10	0	99	7

(b) In order to achieve isothermal TG, different heating algorithms can be applied for heating micrometer sized samples. The absolute temperature and ramp rate can be controlled by different techniques (or a combination), such as pulse width modulation (PWM), On-Off, Proportional integral (PI) & Proportional integral derivative (PID) modes [58-61], by adaption of the number of heat pulses n_{hp} with the

Accepted Manuscript

feedback of temperature sensor. More specifically, when a mass loss is measured then V_{hp} is kept constant until no mass loss can be detected. A constant temperature can then be maintained across the platform, which in turn can be utilized for realizing isothermal TG with microcantilevers. This step will require in-depth calibration of in-built microheaters with temperature.

Thus, the fundamental issues which we discussed above needs to be addressed in order to realize an accurate TG with microcantilevers mimicking the results of conventional & commercial TG.

6. Summary

We have designed, fabricated and calibrated an MMTG device. The performance was tested with 527 ng of $CuSO_4.5H_2O$. The mass sensitivity of the MMTG device was found to be 0.89 pg/Hz by measuring the thermomechanical noise spectra. This way we removed the need of actuation and glue to fix the samples on the device. Thus, there is an improvement in the minimum sample mass handling as well as mass resolution compared to commercial TG. However, non-uniform temperature profile across the platform, inhomogeneous heating of the entire sample and non-isothermal condition in the heater platform along with sample was found to be the limiting factor for high quality TG. The latter needs to be improved significantly to make MMTG a commercially viable technology. One way could be to fabricate bulk microheaters which have shown to better perform in FE simulations compared to the metallic microheaters. Apart from Poly-Si, the material for bulk microheaters could be HfB_2 [62], SiC [62] & SnO_2:Sb [63] which are shown to be capable of operating at high temperatures. We believe the concepts introduced and efforts made in the past for the realization of isothermal TG on commercial TG instruments for increased temperature and mass resolution, needs to be revisited in the case of microcantilevers based TG [52-53]. We aim in future work to address these inherent limitations of performing micro/nano TG with microcantilevers.

Acknowledgement

We would like to thank DST & DFG (BE 3286/4-1) for funding this research work and Ministry of Electronics and Information Technology (MeitY), Government of India. We would like to acknowledge Uwe Rietzler, Maren Müller, Helma Burg for the technical support and Hans Jürgen Butt for fruitful discussion. We would like to thank Polytec team at Waldbronn, Germany for the measurement support.

Author Contributions: "VRR, RB, FN conceived the idea. NT designed, fabricated the device, and executed the experiments, simulations; NT, MZ, EB, FM executed the TG measurements at Polytec; HK, NT, MZ executed IR measurements; NT & RB analysed the data. NT wrote the paper. RB, AL, FN & VRR contributed in active discussion during writing the paper. All authors have internally reviewed the paper."

References

[1] Gao H, Amman J, Lyu X, Woellenstein J, Palzer S 2018 Novel method for thermal characterization of MEMS *J. Microelectromech. Syst.* 27 521-528.

[2] Bazaei A, Zhu Y, Moheimani R, Yuce M R 2012 Analysis of nonlinear phenomena in a thermal micro-actuator with a built-in thermal position sensor *IEEE Sens. Journ.* 12 1772-1784.

[3] Miralles V, Huerre A, Malloggi F, Jullien M-C 2013 A review of heating and temperature control in microfluidic systems: techniques and applications *Diagnostics* 3 33-67.

[4] Toffoli V, Carrato S, Lee D, Jeon S, Lazzarino M 2013 Heater-integrated cantilever for nano-samples thermogravimetric analysis *Sens.* 13 16657-16671.

[5] TA Instruments. [Online]. Available: http://www.tainstruments.com/tga-5500/

[6] Matyszewska D, Napora E, Zelechowska K, Biernat J F, Bilewicz R 2018 Synthesis, characterization, and interactions of single-walled carbon nanotubes modified with doxorubicin with Langmuir-Blodgett biomimetic membranes *J. Nanopart. Res.* 20: 143.

[7] Koutu V, Ojhab P, Shastri L, Malik M M 2018 Study of the effect of temperature gradient on the thermal and electrical properties of ZnO nanoparticles *AIP Conf. Proc.* 1953 030278,.

[8] Membere E, Sallis P 2018 Thermochemical characterization of brown seaweed, Laminaria digitata from UK shores *Journ. of anal. and appl. pyroly.* 131 42-51.

[9] Natalio F, Corrales T P, Panthoefer M, Schollmeyer D, Lieberwirth I, Mueller W E G, Kappl M, Butt H J, Tremel W 2013 Flexible minerals: self-assembled calcite spicules with extreme bending strength *Science* 339 1298-1302.

[10] Natalio F, Corrales T P, Wanka S, Zaslansky P, Kappl M, Lima H P, Butt H J, Tremel W 2015 Siliceous spicules enhance fracture-resistance and stiffness of pre-colonial Amazonian ceramics *Sci. Rep.* 5 13303.

[11] Ihms E C, Brinkman D W 2004 Thermogravimetric analysis as a polymer identification technique in forensic applications *J. Forensic Sci.* 49 505-510.

[12] Gysin U, Rast S, Ruff P, Meyer E, Lee D W, Vettiger P, Gerber C 2004 Temperature dependence of the force sensitivity of silicon cantilevers *Phys. Rev. B.* 69 045403.

[13] Sandberg R, Svendsen W, Molhave K, Boisen A 2005 Temperature and pressure dependence of resonance in multi-layer microcantilevers *J. Micromech. Microeng.* 15 1454-1458.

[14] Thundat T, Wachter E A, Sharp S L, Warmack R J 1995 Detection of mercury vapour using resonating microcantilevers *Appl. Phys. Lett.* 66 1695.

[15] Gimzewski J K, Gerber Ch, Meyer E, Schlittler R R 1994 Observation of a chemical reaction using a micromechanical sensor *Chem. Phys. Lett.* 217 589-594.

[16] Fritz J *et al.* 2000 Translating biomolecular recognition into nanomechanics *Science* 288 316-318.

[17] Chen Z, Zhao F 2014 Single crystalline 4H-polytype silicon carbide microresonator sensor for mass detection *Mater. Lett.* 128 64-67.

Accepted Manuscript

[18] Ilic B, Craighead H G, Krylov S, Senaratne W, Ober C, Neuzil P 2004 Attogram detection using nanoelectromechanical oscillators *Journ. of Appl. Phys*. 95 3694.

[19] Yang Y T, Callegari C, Feng X L, Ekinci K L, Roukes M L 2006 Zeptogram-scale nanomechanical mass sensing *Nanolett.* 6 583-586.

[20] Berger R *et al.* 1998 Micromechanical thermogravimetry *Chem. Phys. Lett.* 294 363-369.

[21] Berger R, Fabian J H 2002 Thermal analysis of nanogram quantities using a micromechanical cantilever sensor *Proc. of NATAS 2002 conference* Pittsburgh USA Sept. 23-25 68-73.

[22] Scandella L. *et al.* 1998 Micromechanical thermal gravimetry performed on one single zeolite crystal *Helv. Phys. Acta* 71 S3-S4.

[23] Ono T, Esashi M 2004 Mass sensing with resonating ultra-thin silicon beams detected by a double-beam laser Doppler vibrometer *Meas. Sci. Technol.* 15 1977-1981.

[24] Lee J, King W P 2007 Microcantilever hotplates: design, fabrication and characterization *Sens. & Act. A* 136 291-298.

[25] Lee J, King W P 2008 Microthermogravimetry using a microcantilever hotplate with integrated temperature-compensated piezoresistive strain sensors *Rev. Sci. Instrum* 79 054901.

[26] Mahmoodi S N, Daqaq M F, Jalili N 2009 On the nonlinear-flexure response of piezoelectrically driven microcantilever sensors *Sens. & Act. A* 153 171-179.

[27] Lee D, Park Y, Cho S-H, Yoo M, Jung N, Yun M, Ko W, Jeon S 2010 Microthermogravimetry of a single microcapsule using silicon microresonators *Anal. Chem.* 82 5815-5818.

[28] Iervolino E, van Herwaarden A W, van der Vlist W, Sarro P M 2011 MEMS for thermogravimetry: fully integrated device for inspection of nanomasses *J. Microelectromech. Syst.* 20 1277-1286.

[29] Voiculescu I, Liao M, Zakerin M, Berger R, Ono T, Toda M 2018 Pico-thermogravimetric material properties analysis using diamond cantilever beam *Sens & Act. A* 271 356-363.

[30] Abedinov N, Grabiec P, Gotszalk T, Ivanov Tz, Voigt J, Rangelow I W 2001 Micromachined piezoresistive cantilever array with integrated resistive microheater for calorimetry and mass detection J. Vac. Sci, Technol. A 19 2884-88

[31] Kshirsagar A, Nyaupane P, Bodas D, Duttagupta S P, Gangal S A 2011 Deposition and characterization of low temperature silicon nitride films deposited by inductively coupled plasma CVD *Appl. Surf. Sci.* 257 5052-5058

[32] Zhou H, Elgaid K, Wilkinson C, Thayne I 2006 Low-hydrogen-content silicon nitride deposited at room temperature by Inductively coupled plasma deposition *Japan. Journ. Appl. Phys.* 45 8388-8392

[33] Tiggelaar R M 2004 Silicon-based microreactors for high-temperature heterogeneous partial oxidation reactions Ph.D. dissertation, Univ. of Twente, Enschede, The Netherlands.

[34] Handbook of silicon based MEMS materials and technologies 2nd edition 2015 Micro and Nano Technologies 124-205 DOI: https://doi.org/10.1016/B978-0-323-29965-7.00006-3.

[35] Zhao J, Gao R, Liu S, Huang Y 2014 A new sensitivity-improving method for piezoelectric resonance mass sensors through cantilever cross-section modification *IEEE Trans. on Industr. Electron*. 61 1612-1621.

[36] Mele L, Santagata F, Iervolino E, Mihailovic M, Rossi T, Tran A T, Schellevis H, Creemer J F, Sarro P M 2012 A molybdenum MEMS microhotplate for high-temperature operation *Sens. & Act. A* 188 173-180.

[37] Guereca R G 2007 Explosive vaporization in microenclosures and boiling phenomena on submicron thin film strip heaters Ph.D. dissertation ETH Zurich Switzerland.

[38] Pulavarthy R A, Alam M T, Haque M A 2014 Effect of heated zone size on micro and nanoscale convective heat transfer *Int. Commun. Heat and Mass Transf*. 52 56-60.

[39] Nelson B A, King W P 2007 Temperature calibration of heated silicon atomic force microscope cantilevers *Sens. & Act. A* 140 51-59.

[40] Briand D, van der Schoot B, de Rooij N F, Sundgren H, Lundstorm I 2000 A low power micromachined MOSFET gas sensor *J. Microelectromech. Syst*. 9 303-308.

[41] Briand D, Krauss A, van der Schoot B, Weimer U, Barsan N, Gopel W, de Rooij N F 2000 Design and fabrication of high-temperature micro-hotplates for drop-coated sensors *Sens & Act B.* 68 223-233.

[42] Bhattacharya P 2014 Technological journey towards reliable microheater development for MEMS gas sensors: A review *IEEE Trans. on Dev. & Mater. Reliab.* 14 589-599.

[43] Kang J, Park J, Park K, Shin J, Lee E, Noh S, Lee H 2017 Temperature control of micro heater using Pt thin film temperature sensor embedded in micro gas sensor *Micro and Nano Syst. Lett.* 5:26.

[44] Spruit R J, Omme J T V, Ghatkesar M K, Garza H H P 2017 A review on development and optimization of microheaters for high-temperature *in situ* studies *J. Microeclectromech. Syst.* 26 1165-1182.

[45] Kralik T, Musilova V, Hanzelka P, Frolec J 2016 Method for measurement of emissivity and absorptivity of highly reflective surfaces from 20K to room temperatures *Metrologia* 53 743-753.

[46] Biro F, Hajnal Z, Duesco C, Barsony I 2017 The critical impact of temperature gradients on Pt filament failure *Microelec. Reliabil.* 78 118-125.

[47] Margaretta D O, Lestari M S, Nuryadin B W, Abdullah M A new criterion for melting of nanostructures of arbitrary shapes *Eur. Phys. J. B.* 89 154.

[48] Abdullah M, Khairunnisa S, Akbar F 2016 Zipper model for the melting of thin films *Eur. J. Phys.* 37 015501.

[49] Polytec MSA-100-3D Microsystem Analyzer [Online]. Available: https://www.polytec.com/eu/vibrometry/products/microscope-based-vibrometers/msa-100-3d-micro-system-analyzer/

[50] Dr. Ilka Kunert, "Thermische analyse und thermodynamische analyse der Phasenbildung", Seminar Anorganische Chemie II, Technische Universität Dresden, Dresden, 19-Apr-2016, Slide number 21 [Online]. Available: http://docplayer.org/17329653-Thermische-analyse-und-thermodynamische-analyse-der-phasenbildung.html

[51] White R L 2012 Variable temperature infrared study of copper sulphate pentahydrate dehydration *Thermochim. Acta* 528 58-62.

[52] Paulik F, Paulik J 1972 Kinetic studies of thermal decomposition reactions under quasi-isothermal and quasi-isobaric conditions by means of the derivatograph *Thermochim. Acta* 4 189-198.

Accepted Manuscript

[53] Paulik J, Paulik F 1971 Quasi-isothermal thermogravimetry *Anal. Chim. Acta* 56 328-331.

[54] Tian W C, Chan H K L, Lu C J, Pang S W, Zellers E T 2005 Multiple-stage microfabricated preconcentrator-focuser for micro gas chromatography system *J. Microelectromech. Syst*. 14 498-507.

[55] Yeom J, Field C R, Bae B, Masel R I, Shannon M A 2008 The design, fabrication and characterization of a silicon microheater for an integrated MEMS gas preconcentrator *J. Micromech. Microeng*. 18 125001 (12pp).

[56] Hwang W-J, Shin K-S, Roh J-H, Lee D-S, Choa S-H 2011 Development of micro-heaters with optimized temperature compensation design for gas sensors *Sens.* 11 2580-2591.

[57] Yao Y, Fu K K, Yan C, Dai J, Chen Y, Wang Y, Zhang B, Hitz E, Hu L 2016 Three-dimensional printable high-temperature and high-rate heaters *ACS Nano* 10 5272-5279.

[58] Gardner J W, Guha P K, Udrea F, Covington J A CMOS interfacing for integrated gas sensors: a revie *IEEE Sens. Journ.* 10 1833-1848.

[59] Low H M, Tse M S, Chiu M M 1998 Thermal induced stress on the membrane in integrated gas sensor with micro-heater *Proc. of the IEEE Hong Kong Electron Devices Meeting* 140-143.

[60] Rastrello F, Placidi P, Scorzoni A 2011 A system for the dynamic control and thermal characterization of ultra low power gas sensors *IEEE Trans. Instrum. Meas.* 60 1876-1883.

[61] Sharma D K, Dwara R S V, Botre B A, Akbar S A 2017 Temperature control and readout circuit interface for MOX based NH_3 gas sensor *Microsyst. Technol*. 23 1575-1583.

[62] Solzbacher F, Imawan C, Steffes H, Obermeier E, Moller H 2000 A modular system of SiC-based microhotplates for the application in metal oxide gas sensors *Sens. & Act. B* 64 95-101.

[63] Spannhake J, Schulz O, Helwig A, Krenkow A, Mueller G, Doll T 2006 High-temperature MEMS heater platforms: long-term performance of metal and semiconductor heater materials *Sensors* 6 405-419.

Accepted Manuscript